MAE 598 – Applied Computational Fluid Dynamics, Fall 2018 – Dr. Huang

Marielle Debeurre

Project #4

Collaboration Statement
Collaborator: Anna Hu

1. Boolean geometry subtraction (Tasks 2 and 3)	Help was received on creating the boolean "subtraction" feature in geometry, necessary to build the complex and integrated 3D systems in Tasks 2 and 3
2. Pressure/velocity effect on drag force discussion (Task 3b)	The collaborators discussed the behavior of the systems between Task 3a and 3b in order to come up with an explanation for the pressure and velocity effects on the drag force
3. General comparison of results (All tasks)	A general comparison of results was made for all tasks to see if simulation results matched between collaborators
4. Period/amplitude of oscillation (Task 1c)	Help was needed on finding the period and amplitude of oscillation in Task 1c, which did not agree between collaborators until several runs were conducted

Task 1

(a) In this task, a simulation of water flow over a cylinder was run using a 2D system of a circular disk placed within the domain of the water flow, as shown below. The domain constraints were given in units of cm, with the left boundary being the velocity inlet of the water and the right boundary being the outlet. The other boundaries in the system were denoted as walls. The simulation was run using a laminar model and a transient solution was sought using a time step of 0.5 sec for 7200 time steps with 10 max iterations per time step. The unique feature in this task was that the inlet velocity was set to 0.3 cm/s in the positive x-direction (the direction normal to the boundary), and the transient simulation was run for a full hour (0.5 sec · 7200 = 3600 sec = 1 hr).

(i) The Reynolds number for this case was calculated based on the properties of the fluid, taken from the Fluent database, and the geometry of the system. The density of water and dynamic viscosity were given as $\rho = 998.2$ kg/m^3 and $\mu = 0.001003$ kg/m·s, respectively. The length used in the calculation, which was equal to the diameter of the circular disk, was also given as $d = 0.1$ m. The inlet velocity of the system was set to $U = 0.003$ m/s for this case. The calculation of the Reynolds number is as follows:

$$Re = \frac{UL\rho}{\mu} = \frac{(0.003\,\frac{m}{s})(0.1\,m)(998.2\,\frac{kg}{m^3})}{0.001003\,\frac{kg}{m\cdot s}} = 298.564$$

A Reynolds number of 298.564 likely falls within the "transition" zone between laminar and turbulent flow, but is much closer to the laminar end of the spectrum than the turbulent zone.

(ii) The following contour plots show the x-velocity and static pressure distributions over the flow domain at time t = 1 hr. As is expected, some oscillations do occur behind the cylinder, as the flow was found to be not perfectly laminar.

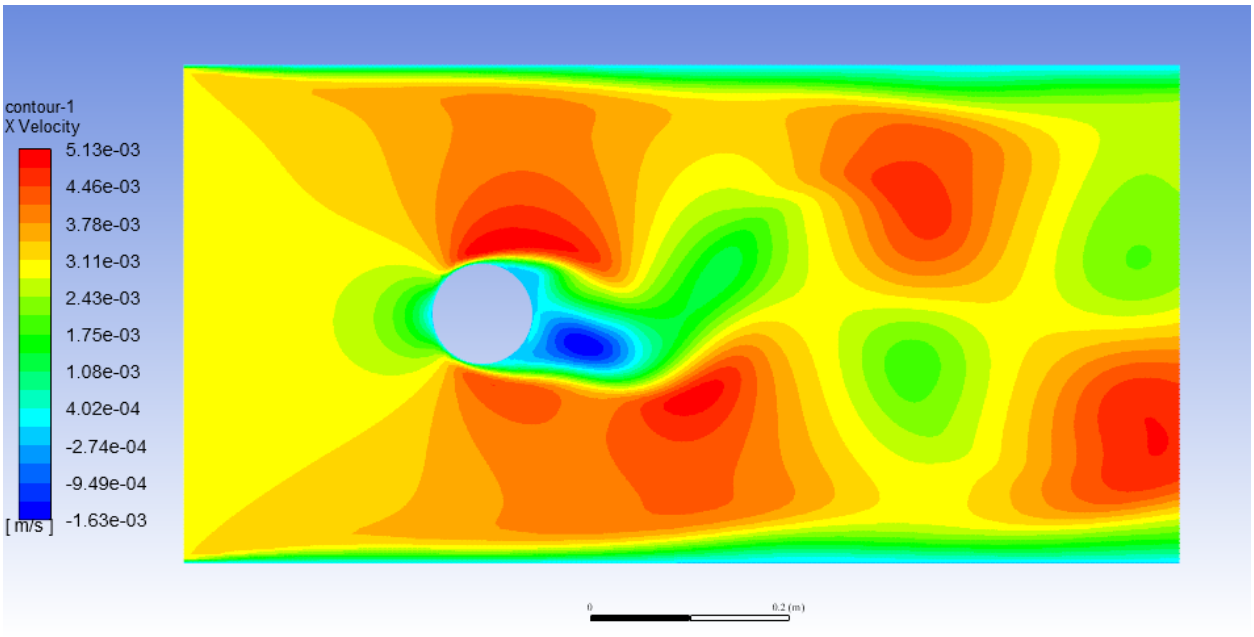

Figure 1: X-Velocity at t = 1 hr

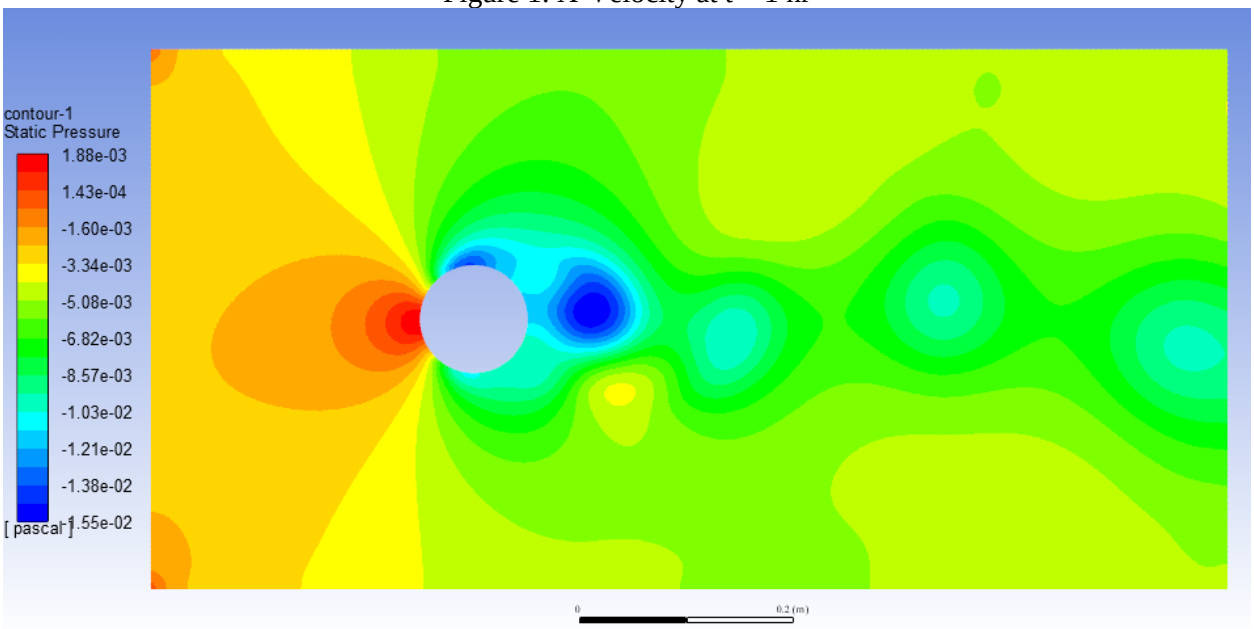

Figure 2: Static Pressure at t = 1 hr

(b) This task repeated the simulation in Task 1a, but with the inlet velocity changed to 2 cm/s in the positive x-direction, which meant a much faster inlet velocity than in the first simulation. The Reynolds number was expected to increase to go along with the increased flow velocity; this number is calculated below. The simulation was also run for a full hour, with a report file measuring values of the lift coefficient over the simulation, which was necessary for part (iii).

(i) The Reynolds number for this case was calculated in the same manner as in Task 1a. The fluid remained the same, so the properties of water were left as the same: density, $\rho = 998.2$ kg/m^3 and dynamic viscosity, $\mu = 0.001003$ kg/m·s. The geometry of the system did not change, so the diameter of the cylinder was the same at $d = 0.1$ m. Only the inlet velocity changed between Tasks 1a and 1b, with U =

0.02 m/s in Task 1b. Using these parameters, the Reynolds number for this case was calculated as shown:

$$Re = \frac{UL\rho}{\mu} = \frac{(0.02\,\frac{m}{s})(0.1\ m)(998.2\,\frac{kg}{m^3})}{0.001003\,\frac{kg}{m\cdot s}} = 1990.429$$

This Reynolds number is much higher than in Task 1a. While it may still be within the loosely-defined "transition" zone between laminar and turbulent flow, it is much closer to a turbulent flow than in Task 1a.

(ii) The contour plots below mirror those in Task 1a, showing x-velocity and static pressure over the domain at t = 1 hr. As noted above, the oscillations, especially in the x-velocity plot, are wider than in Task 1a, due to the higher inlet velocity and Reynolds number. The oscillations retain the same pattern as in Task 1a, however, which is likely due to this simulation also being mostly within the Reynolds number "transition" and oscillatory period (i.e., it is not an explicitly turbulent and chaotic flow).

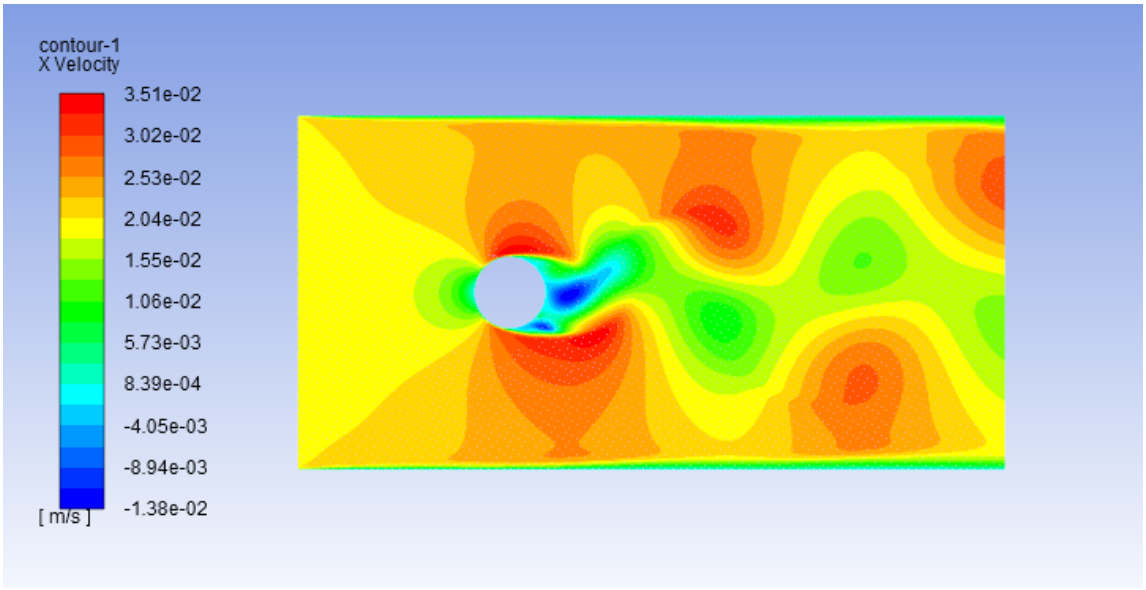

Figure 3: X-Velocity at t = 1 hr

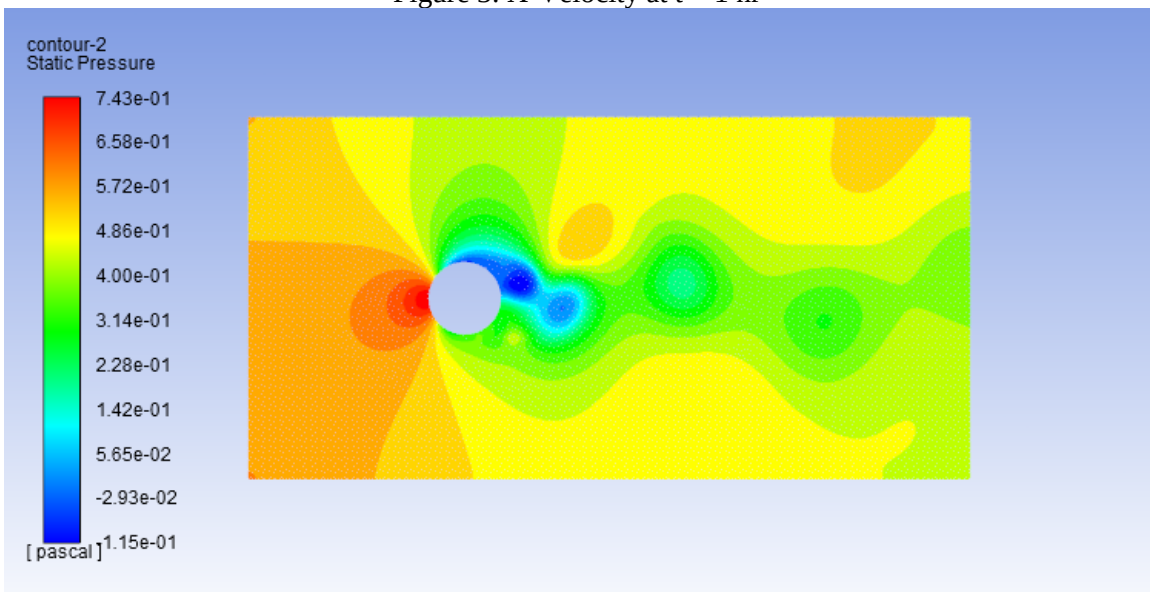

Figure 4: Static Pressure at t = 1 hr

(iii) For this simulation, a report file was also generated to monitor the lift coefficient as a function of the flow time as it oscillated for the duration of the hour-long simulation. The lift coefficient could then be plotted over the last 10 minutes of the simulation, from t = 50 min to t = 1 hr, to ensure that the oscillations in the lift coefficient had converged. The period and amplitude were then determined from the oscillations in the function as shown below:

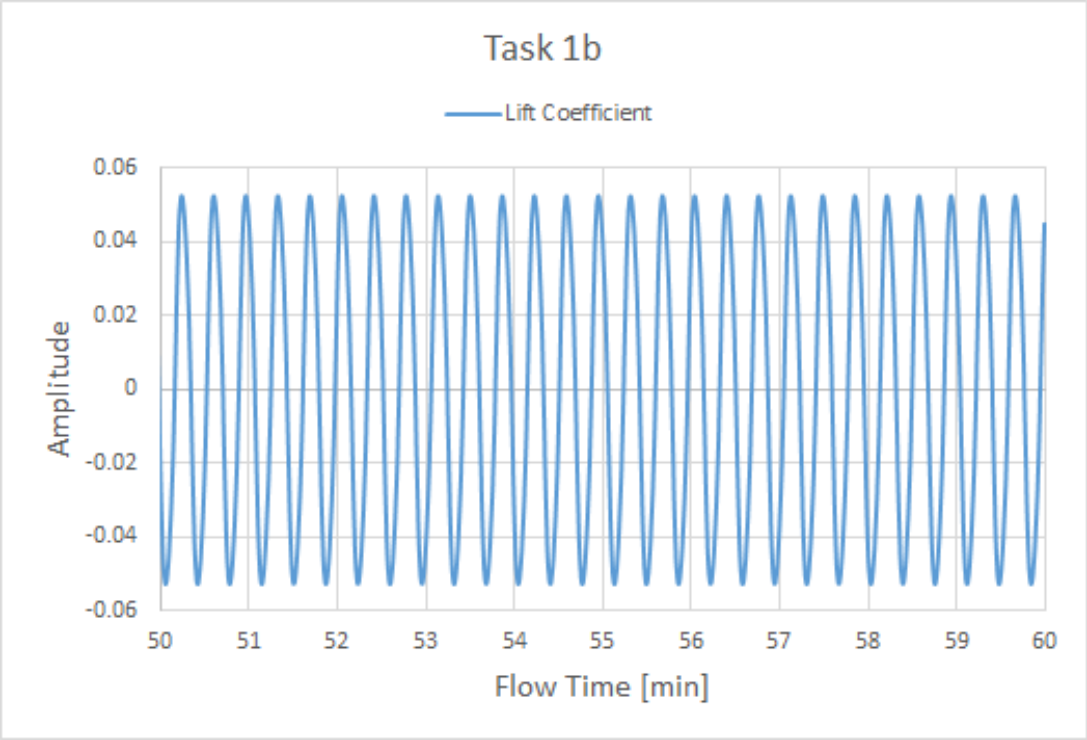

Figure 5: Lift Coefficient as Function of Flow Time at 50 min < t < 1 hr

The period of oscillation was calculated to be around $\tau = 21.5$ sec and the corresponding amplitude of oscillation was found to be $A = 0.0525$.

(c) In this task, the simulations of Task 1b were repeated with the same inlet velocity of 2 cm/s for two separate runs. The unique features in each of these runs were the changes in geometry of the system's 2D representation of the cylinder, from a circular disk to an ellipse. In each run, the geometry of the system was changed and the simulation was run using identical conditions to Task 1b. Descriptions of the geometrical changes for each run are described below.

Run 1: In the first run, the circular disk was altered to an ellipse elongated in the y-direction, with a major and minor axis of 12 and 8 cm, respectively. The simulation was then run exactly as in Task 1b, including the report file that monitored that lift coefficient throughout the flow simulation. This lift coefficient was again plotted as a function of flow time for the last 10 minutes of the simulation, and the oscillations were compared to those produced in Task 1b.

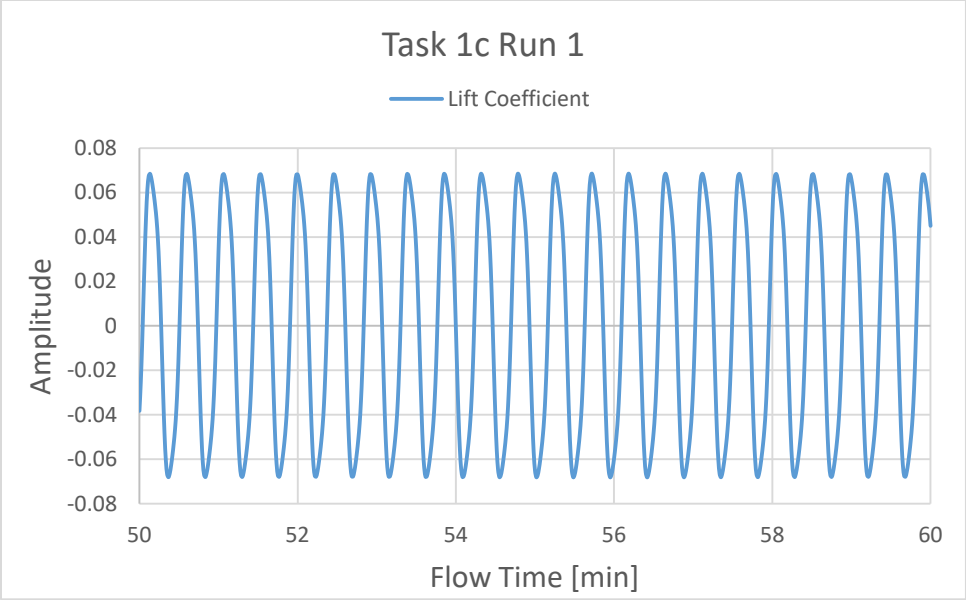

Figure 6: Lift Coefficient as Function of Flow Time at 50 min < t < 1 hr

The period of oscillation was calculated to be around $\tau = 23$ sec for this case, and the amplitude of oscillation was determined to be A = 0.0733. Both the period of oscillation and the amplitude were found to be higher than those of the circular cylinder in Task 1b. A possible explanation for these results could be due to the orientation of the ellipse, as an ellipse elongated in the y-direction would have a greater external cross-sectional area in the path of the fluid flow.

Run 2: In the second run, the same setup as in Task 1b was again used, with the inlet velocity also set as 2 cm/s. For this case, however, the 2D circular disk was converted into an ellipse elongated in the x-direction, with major and minor axes equal to 12 and 8 cm, respectively. The lift coefficient was again monitored as a function of flow time, and the last 10 minutes of the simulation are plotted below. Overall, this run was performed exactly as Run 1, but the orientation of the ellipse was changed from the major axis in the y-direction (Run 1) to in the x-direction (Run 2). The period and amplitude of oscillation could again be determined and compared to those in Task 1b and Run 1 of Task 1c.

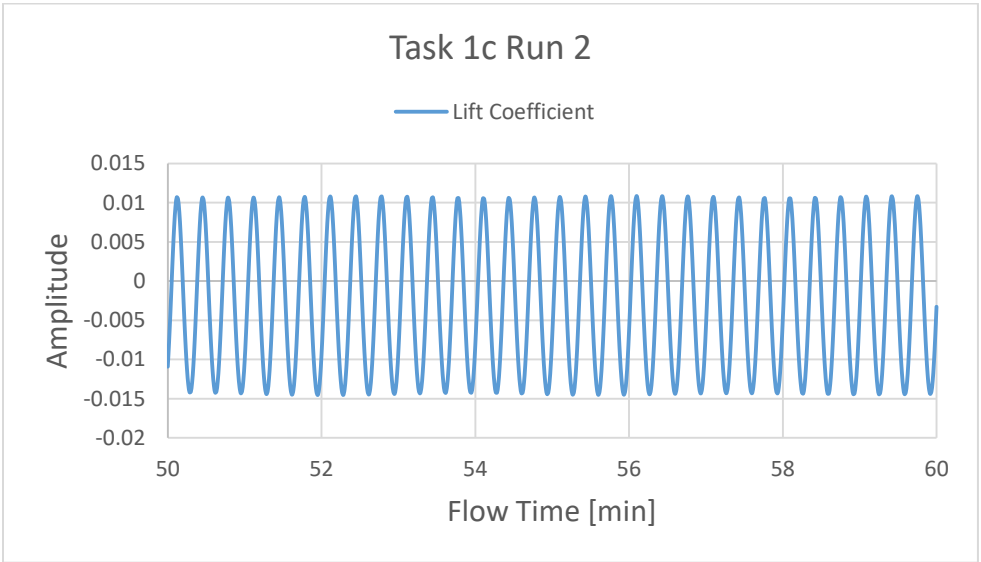

Figure 7: Lift Coefficient as Function of Flow Time at 50 min < t < 1 hr

The period of oscillation was found to be approximately $\tau = 20$ sec and the amplitude of the oscillations was determined to be $A = 0.0125$. Both the period and amplitude of oscillations in this run were found to be less than those found in Task 1b and, consequently, Run 1. Along the same logic as in Run 1, a possible explanation for the decrease in period and amplitude could be due to the orientation of the ellipse being elongated in the x-direction. This shape decreases the overall external cross-sectional area facing the fluid's flow path, which could overall decrease the amplitude of the oscillating lift coefficient.

Task 2

In this task, a flying saucer object was placed in a tunnel filled with air, similar to the external flow of Task 1, but simulated with a 3D air-filled system. The dimensions of the flying saucer, given in cm, were provided, and the cylindrical domain of the 3D system created around it, which can be seen in the figures below. The saucer was "removed" from the tunnel using the unique boolean geometry tool, which separated the flying saucer from the tunnel and allowed Fluent to recognize it as an object in the air flow's path, simulating external flow over the saucer. The left boundary was set as the velocity inlet of the system, while the right boundary was set as the outlet. The remaining boundaries of the domain were set as walls. Unlike Task 1, this simulation employed the turbulence k-epsilon model and a steady solution was sought, usually to 5000 iterations. The inlet velocity was set in Fluent as 50 m/s in the positive x-direction, which equated to the direction normal to the surface of the inlet. This inlet velocity was kept constant even as the title angle, θ, of the flying saucer changed, which represented a rotation around the z-axis of the saucer. Four simulations were run for four different tilt angles: $\theta = 0^{\circ}$, 15°, 30°, and 45°.

(i) The number of elements and nodes were carefully monitored in this task to ensure that they did not exceed the maximum allowable number. The mesh was made as fine as possible given the element constraints. A plot of the mesh along the plane of symmetry for the case of $\theta = 45^{\circ}$ is shown below, detailing how the mesh becomes more precise around the edges of the flying saucer:

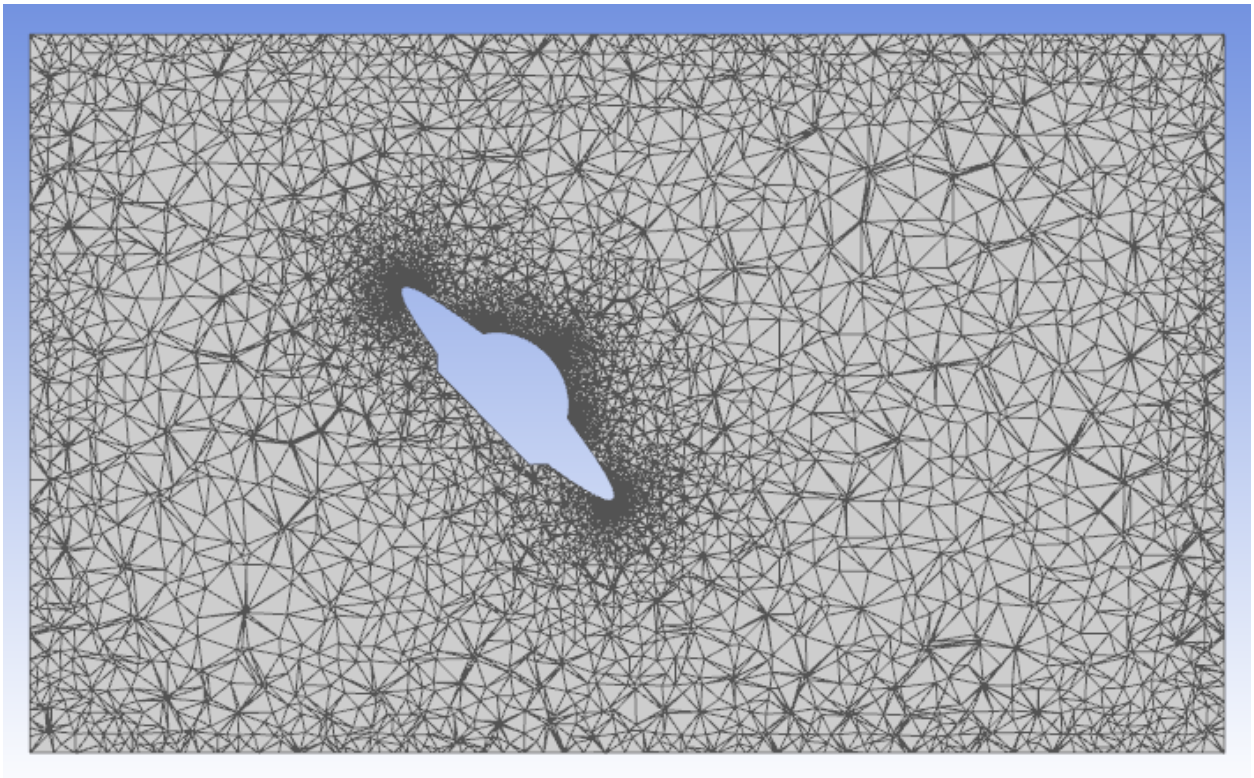

Figure 8: System Mesh along Plane of Symmetry, $\theta = 45^{\circ}$

(ii) Contour plots of the x-velocity along the plane of symmetry were also generated for θ = 0º and 45º to show how the air's velocity was impacted by the obstacle in its path. These contour plots also detail the differences in external flow depending on the tilt angle of the ship; the velocity was only mildly impacted when the ship was perfectly horizontal, but a large tilt in the saucer's angle created a wide gap and slowing of the velocity behind the saucer. This gap appeared like an eddy behind the saucer, with the velocity even pointing in the negative x-direction at some locations behind the ship.

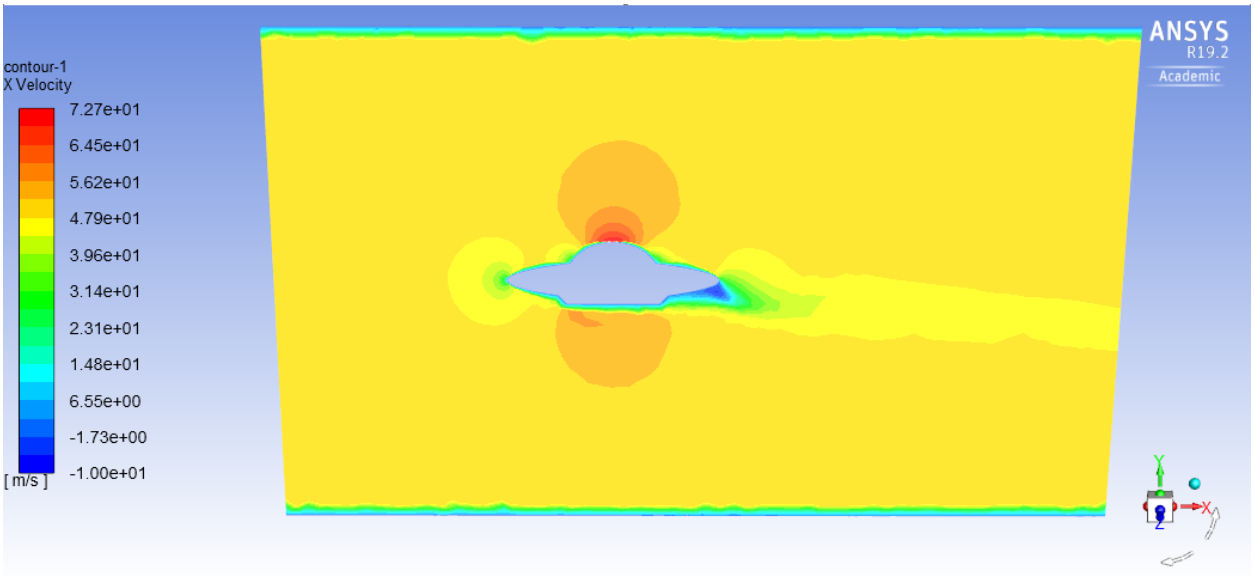

Figure 9: X-Velocity along Plane of Symmetry, θ = 0º

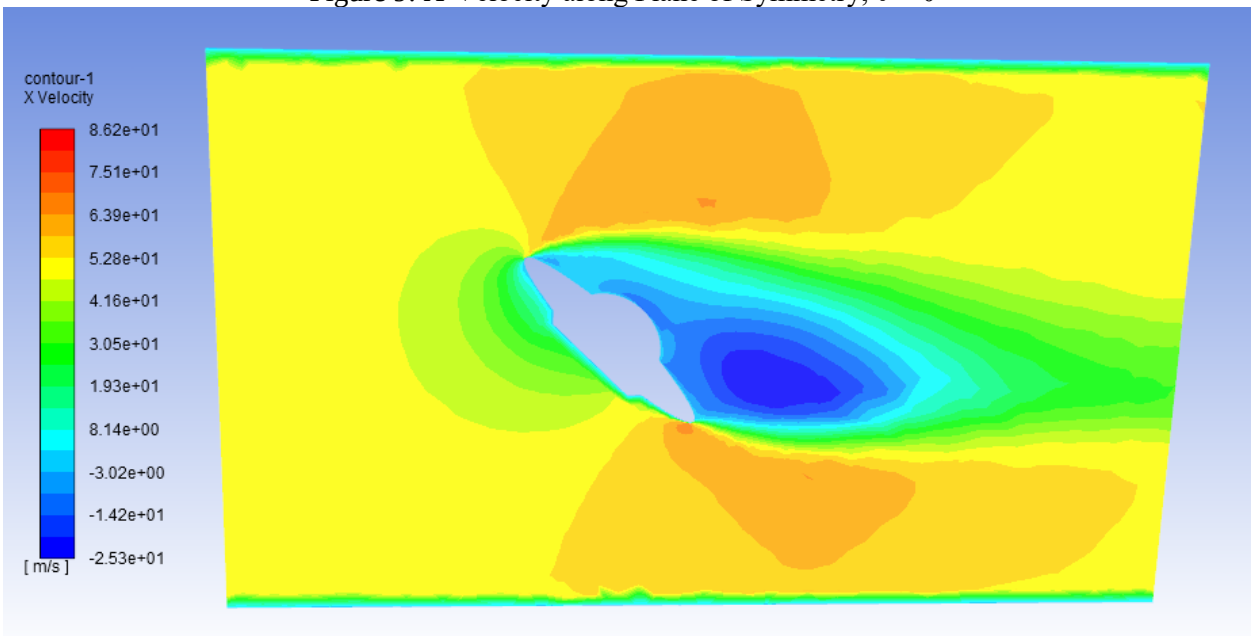

Figure 10: X-Velocity along Plane of Symmetry, θ = 45º

(iii) Another way of determining how the fluid's flow was affected by the tilt angle of the flying saucer was through measuring the lift and drag forces exerted on the ship at each angle. A rough distribution of lift and drag forces as functions of the angle could then be created. As the tilt angle of the flying saucer changed, it created more of a disturbance in the flow, due largely to the increase in the saucer's external surface and cross-sectional area over which the flow passed with each increase in tilt angle. It was

therefore expected that the lift and drag forces would each increase as the tilt angle of the flying saucer increased. For each tilt angle, the lift and drag forces were calculated in Fluent after 5000 iterations, and the values were combined into a table and then plotted as shown below:

Table 1: Lift and Drag Forces for Each θ				
Tilt Angle	0º	15º	30º	45º
Lift Force	21.095 N	117.781 N	140.628 N	121.396 N
Drag Force	10.629 N	27.717 N	87.043 N	174.398 N

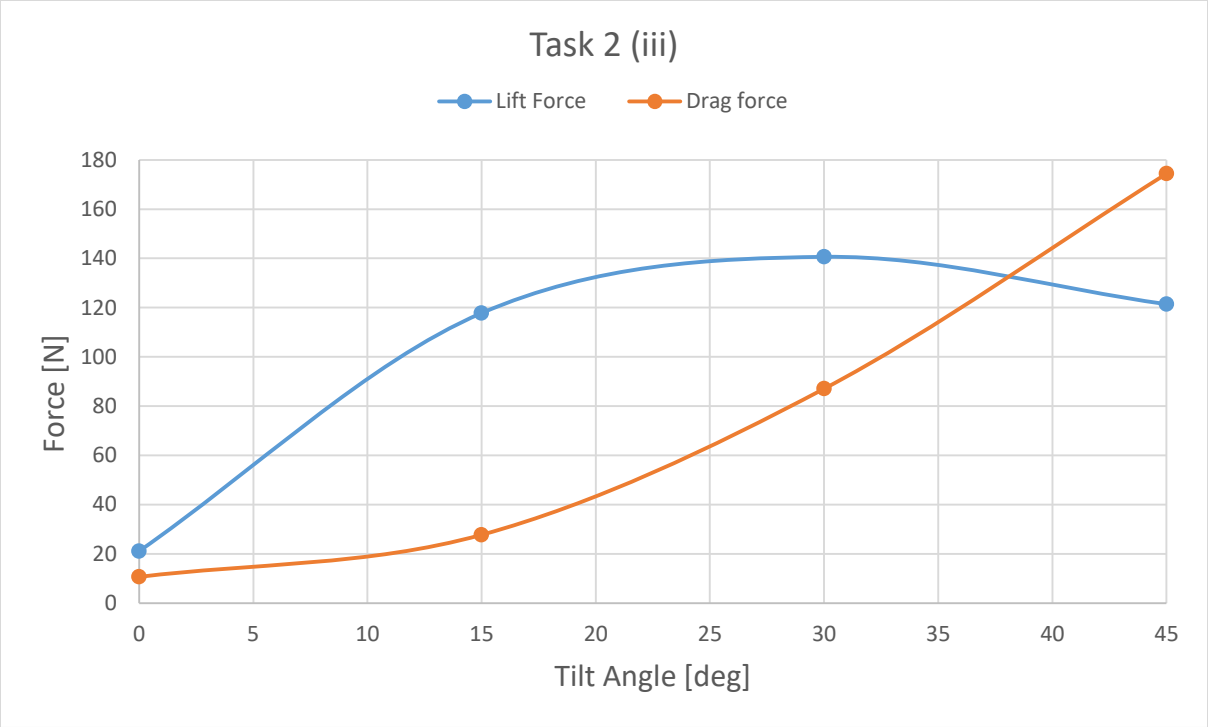

Figure 11: Lift and Drag Forces as Functions of Tilt Angle θ

As hypothesized, the lift and drag forces did increase with increasing tilt angle in general, but there reached a point in the saucer's tilt where the drag force acting on the ship was larger than the lift force. This shift, according to the above plot, occurred somewhere between the 30º and 45º tilt angles, when the lift and drag forces equaled each other and then traded places.

Task 3

(a) Similar to the simulation in Task 2, this task simulated a pentagon-shaped building in a wind tunnel using a 3D geometrical domain filled with air. The building was placed on the "ground" of the rectangular domain, in the center, and the left boundary condition was set as the velocity inlet while the right boundary condition was set at the outflow. The remaining surfaces were labeled as walls. The inlet velocity was set to 50 m/s in the positive y-direction, which equated to the direction normal to the surface of the inlet. This flow inlet was directed towards a flat edge of the pentagon building, which can be seen in the contour plots below. The turbulence k-epsilon model was used for the simulation and a steady solution was sought after 5000 iterations.

(i) The contour plots shown below detail the steady pressure and y-velocity distributions along a horizontal place created with z = 0.5 m. This equated to a plane that cut through the middle of the building and showed the distributions looking down on the top of the building.

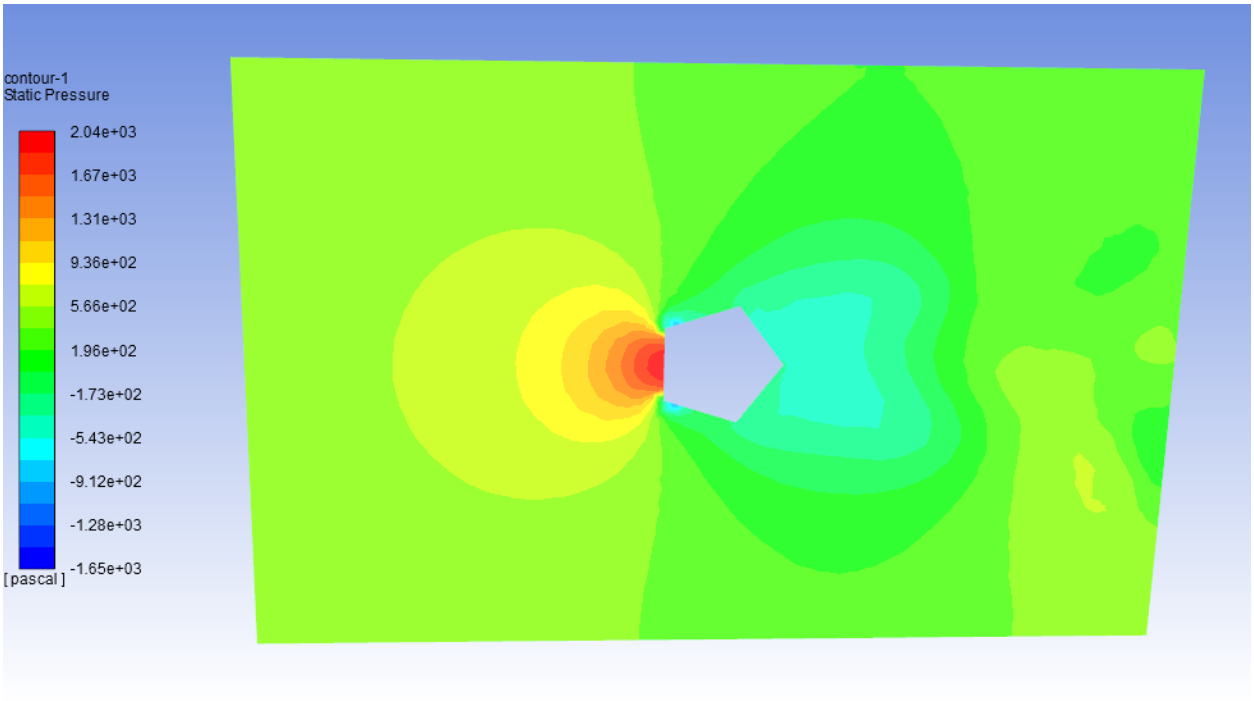

Figure 12: Static Pressure along Horizontal Plane, z = 0.5 m

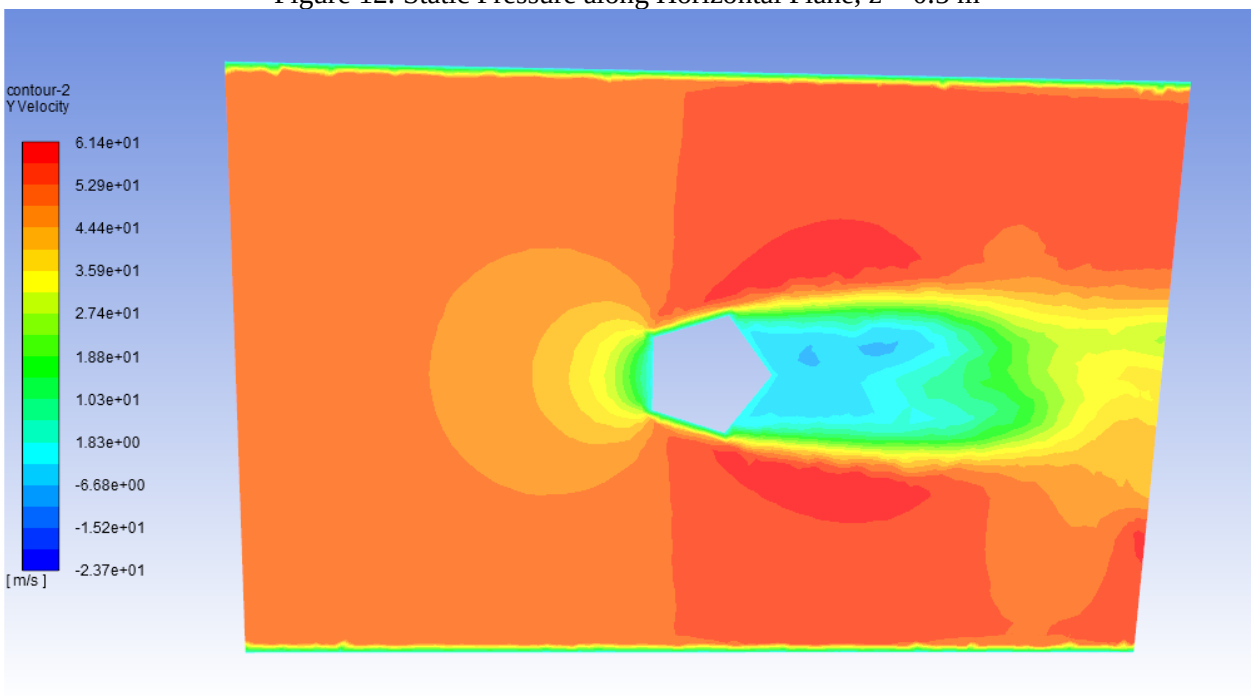

Figure 13: Y-Velocity along Horizontal Plane, z = 0.5 m

(ii) The following contour plot shows the y-velocity distribution along the plane of symmetry, which equated to a side-view y-velocity distribution, as if looking at the building from the side. Similar to the

slower y-velocity and eddying behind the building in Figure 13, the velocity slows and even moves in the negative y-direction in the contour plot shown below:

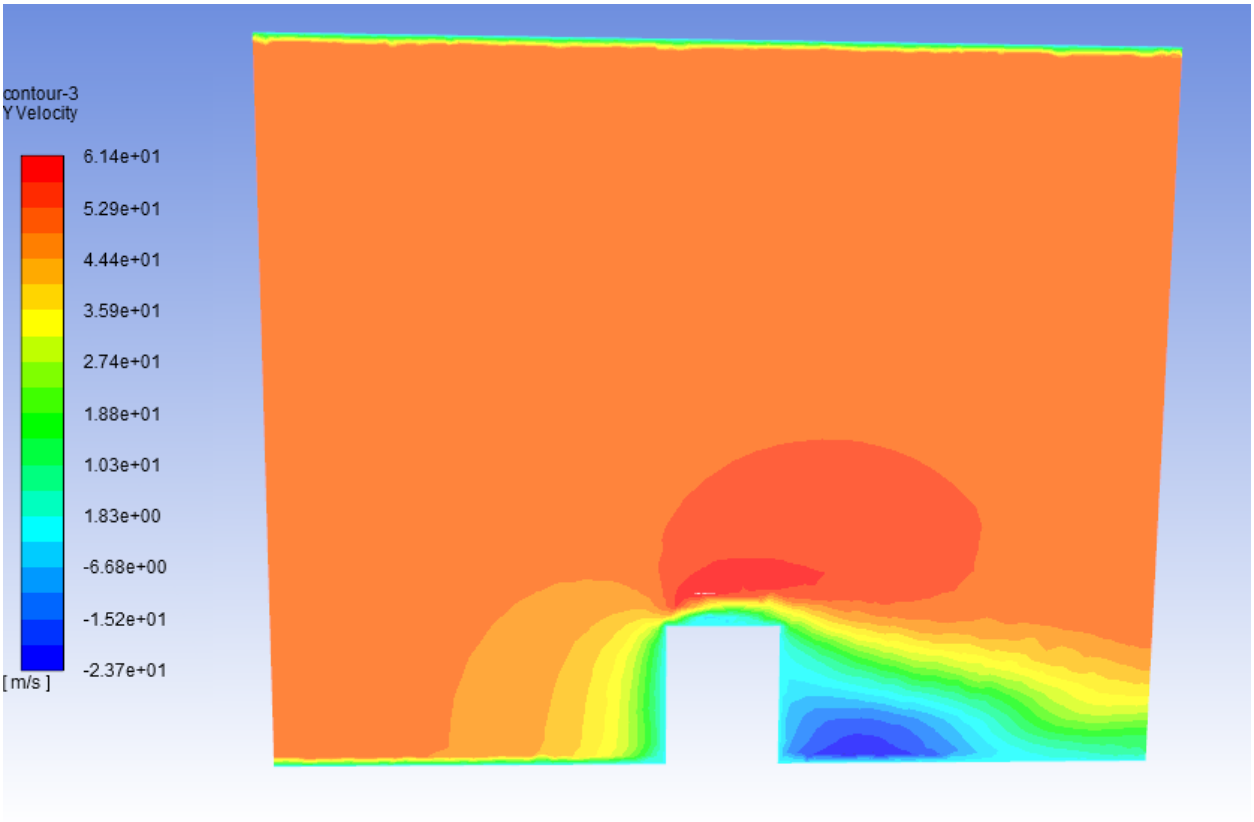

Figure 14: Y-Velocity along Plane of Symmetry

(iii) The value of the total drag force exerted on the building by the fluid was also calculated in Fluent for this simulation. The drag force is composed of two different terms, a pressure term and a viscous term. Each of these contributes to the overall total drag force as shown below:

Total drag force = 930.627 N
Pressure term contribution = 927.666 N
Viscous term contribution = 2.962 N

It can be seen that the viscous term contributes much less to the overall drag force exerted on the building. This makes sense, given that the flow was assumed turbulent (turbulence k-epsilon model was used) and the pressure term dominates over the viscous term in this turbulent model.

(b) In this simulation, the same construction was used, but the wind tunnel was directed at one of the pentagon's vertices instead of one of the flat sides. This simulation was achieved simply by switching the "velocity-inlet" and "outflow" boundaries on the existing geometry and switching the direction of the inlet velocity of 50 m/s to be pointing in the **negative** y-direction, which is the direction normal to the surface of the inlet. For this reason, while the contour plots below are oriented to match the orientation of the contour plots in Task 3a, the coloring is reversed to indicate the negative y-direction inlet velocity.

(i) As in Task 3a, contour plots of steady pressure and y-velocity were created along a horizontal plane with z = 0.5 m. This plane was exactly identical to that used in Task 3a (i). As noted above, the color distribution for the y-velocity contour plot was reversed from that used in Task 3a due to the change in y-

direction inlet velocity. As can be seen from the color distribution, the inlet velocity was set to -50 m/s in the y-direction, or 50 m/s in the negative y-direction. As the geometry of the system was left unchanged and only the boundary conditions were named differently, this meant that the inlet flow velocity had to be reversed to direct the air flow towards the vertex of the pentagon building. Once again, the slowing behind the structure and eddying y-velocity immediately behind it are noted.

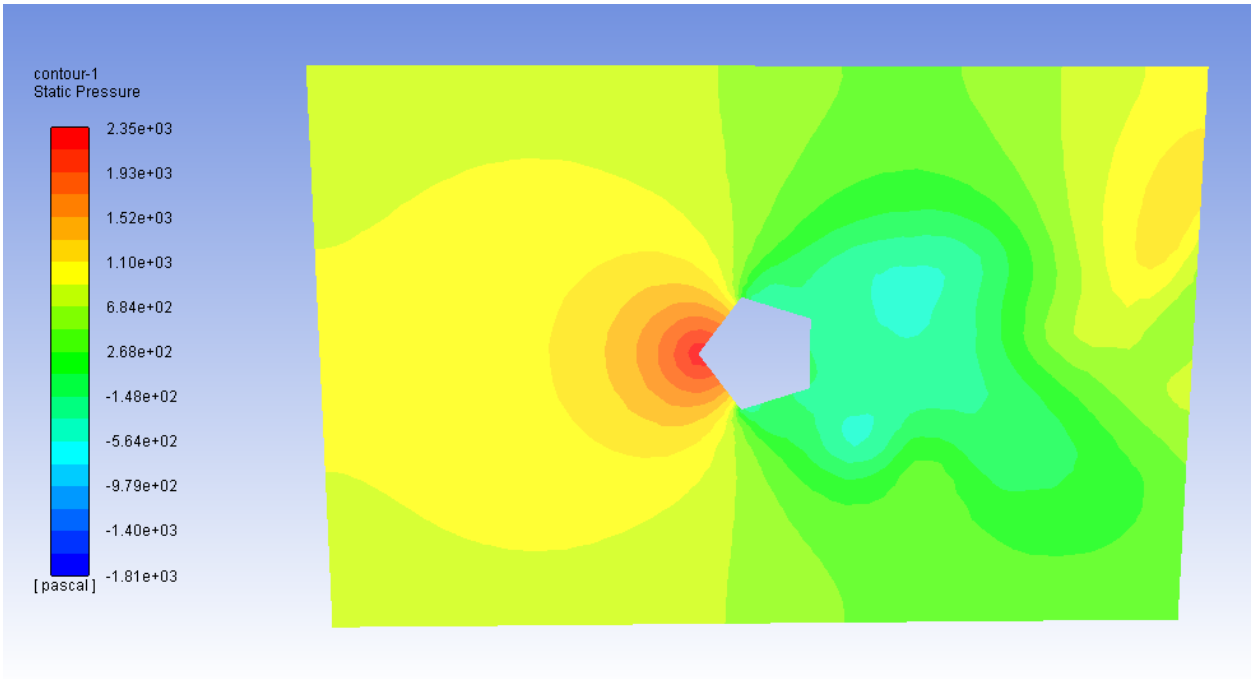

Figure 15: Static Pressure along Horizontal Plane, z = 0.5 m

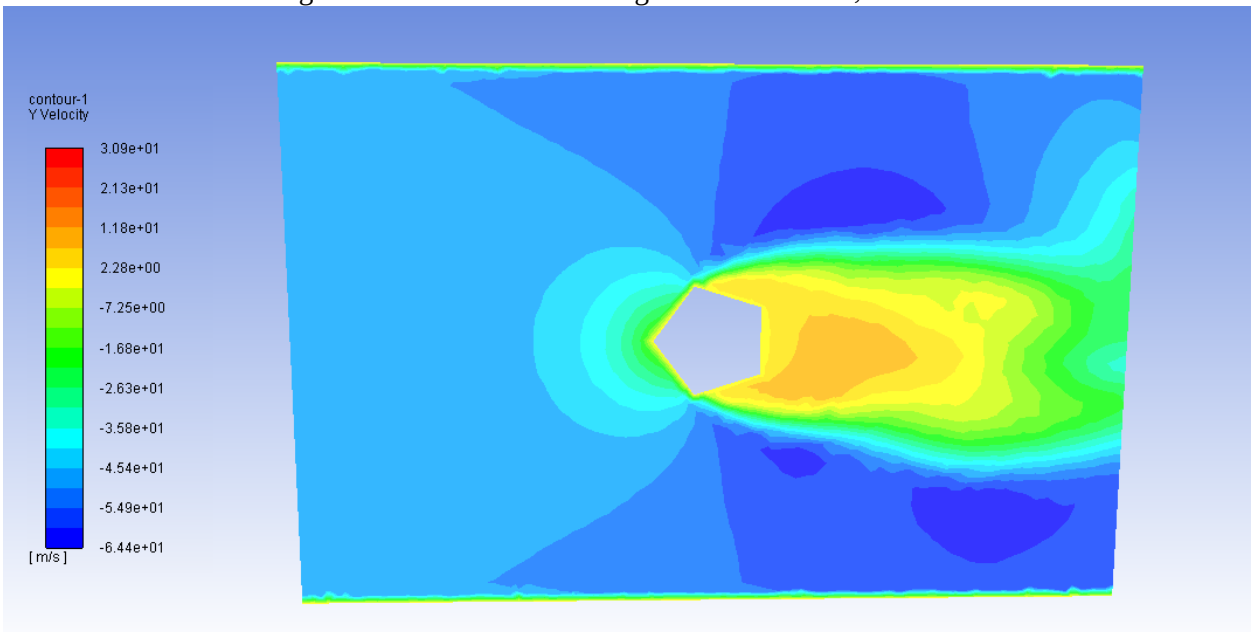

Figure 16: Y-Velocity along Horizontal Plane, z = 0.5 m

(ii) The following contour plot details a “side-view” distribution of y-velocity over the plane of symmetry. As in the previous plot, the color distribution on the plot reflects the reversed inlet velocity of 50 m/s in the negative y-direction. The coordinates originally used to create the structure meant that the

velocity must be negative to point the flow at one of the building's vertices. The following contour plot also shows the interesting slowing and eddying or velocity stagnation directly behind the structure, as was seen in the corresponding plots in Task 3a.

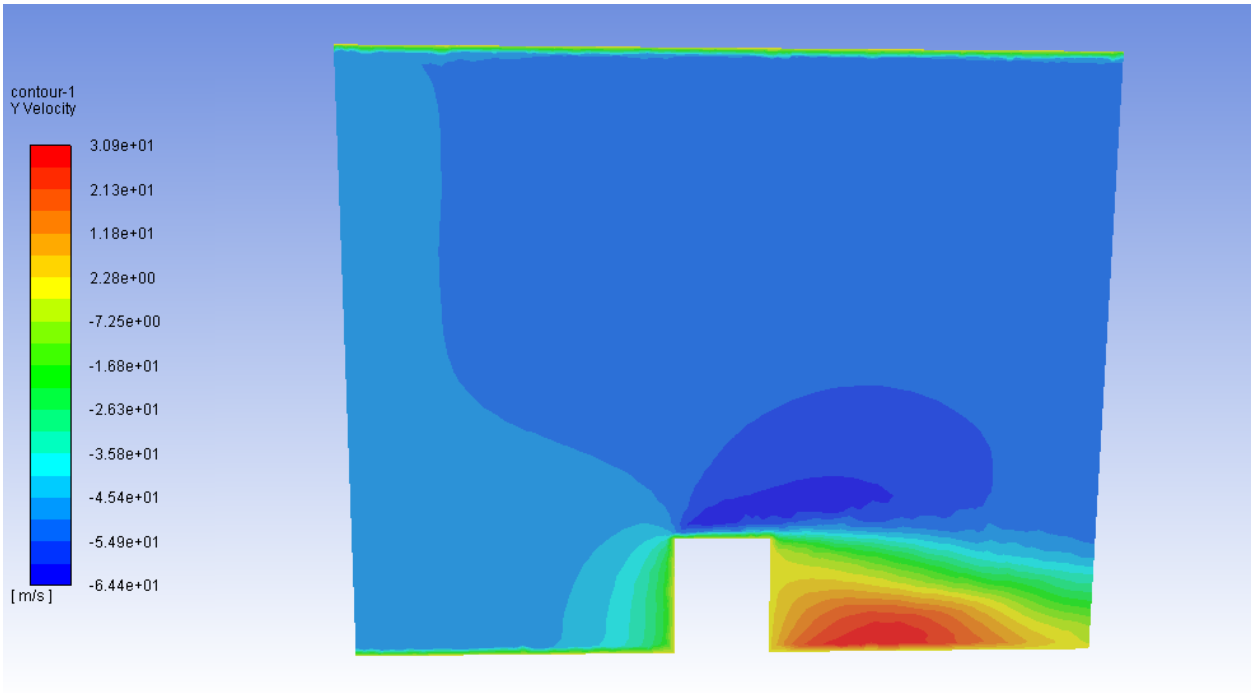

Figure 17: Y-Velocity along Plane of Symmetry

(iii) As in Task 3a, the total drag force was computed in Fluent along with the pressure and viscous contributions to the drag force. The total drag force and its breakdown into the contributions from each term are as follows:

Total drag force = 1379.030 N
Pressure term contribution = 1378.102 N
Viscous term contribution = 0.928 N

The viscous term contribution to the total drag force in this turbulently-modeled system is once again dominated by the pressure term's contribution. However, when comparing the results of the drag force calculations in Tasks 3a and 3b, it can be seen that differences in the pressure and velocity structures due to the change in the building's geometrical structure affect the drag force in each case. While the decomposition of pressure and viscous terms between Tasks 3a and 3b were comparable, with the pressure contribution largely dominating the viscous contribution in each case, the overall value of the drag force was calculated to be much higher when the flow encountered the building's vertex instead of its flat side. The increased drag force in Task 3b was likely due to a number of different explanations. First, the maximum value of static pressure was larger at the pentagon's vertex (3b) than at the pentagon's edge (3a). This is because the first point of contact the flow runs into in the second simulation was the vertex of the pentagon, which has a much smaller cross-sectional area than the edge of the building, and pressure is equal to force divided by the area (↓ area, ↑ pressure). Therefore, the magnitude of pressure distribution at the left half of the building was much larger in Task 3b than the left half of the building in Task 3a. Secondly, the external surface area over which the flow passed was much greater in Task 3b than in Task 3a, as the slanted edges of the building also acted as impediments to the fluid's flow. This decreased the velocity around the edges of the building's slants and increased the "eddying" velocity

behind the building when compared to the contour plots in Task 3a, which increased the drag force very similarly to the behavior of the flying saucer at a tilt angle of 45º in Task 2 (which also resulted in a very high increase in drag force). For these reasons, the drag force in Task 3b was found to be greater than in Task 3a, with the pressure term contribution also playing a larger role in the overall drag force.